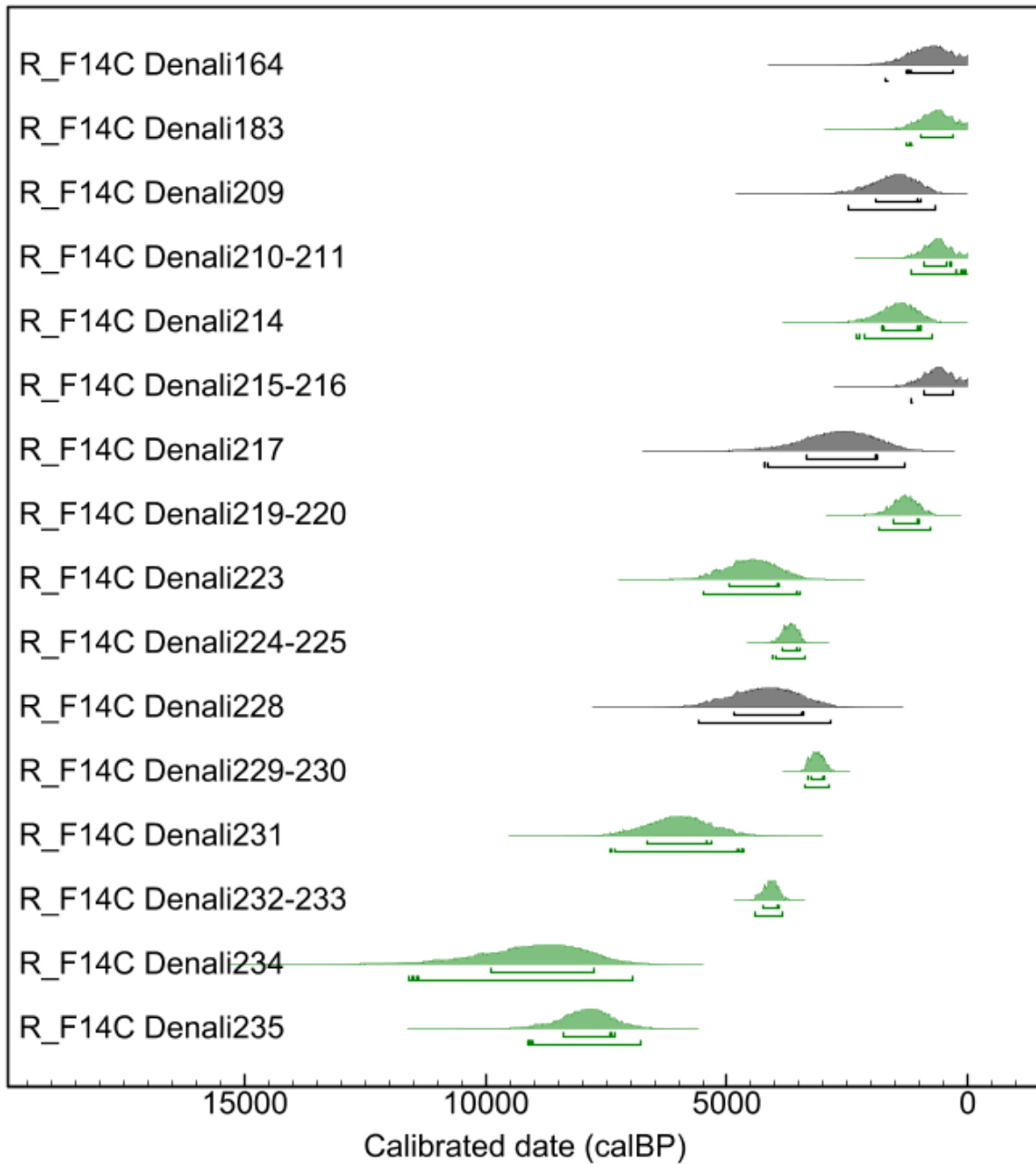
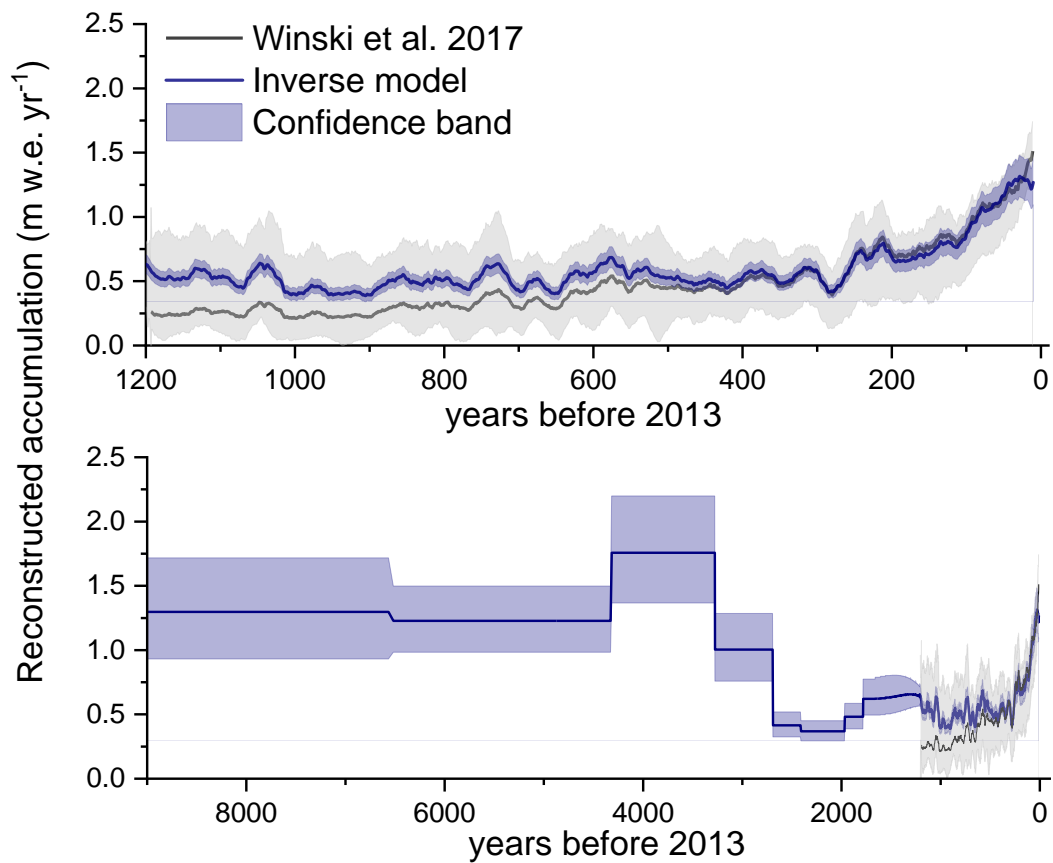


## Supplementary



**Figure S1** Calibrated  $^{14}\text{C}$  ages for all Denali ice core samples as derived in OxCal v4.4.4 using the Northern Hemispheric IntCal20 radiocarbon calibration curve (Ramsey 2021; Reimer et al. 2020). Here, without applying the sequence model (no constraint by assuming sequential ordering of samples). Shown are probability distributions of calibrated dates for samples significantly  $>10 \mu\text{g C}$  (green) and  $<10 \mu\text{g C}$  (grey) for AMS analysis.  $1\sigma$  and  $2\sigma$  ranges of the calibrated ages are indicated by the respective lines below.



**Figure S2** Upper panel: Reconstructed annual net accumulation rates from the inverse model (navy line and shading) compared with reported values, based on a 3D model, from Winski et al. 2017 (black line and shading). Lower panel: Reconstructed accumulation from this study, extended back in time.

**Table S1**  $^{14}\text{C}$  results of all Denali ice core samples, here with calibrated ages (OxCal v4.4.4, IntCal20) as derived if the sequence model is not applied, and also for samples  $< 10 \mu\text{g C}$  (see main text).

Sample ID	AMS Lab ID	Depth (m)	Mid Depth (m w.e.)	Carbon amount ( $\mu\text{g C}$ )	WIOC ( $\mu\text{g kg}^{-1}$ )	$F^{14}\text{C}$ ( $1\sigma$ )	Calibrated $^{14}\text{C}$ age (cal BP, $1\sigma$ range)
Denali164*	BE-10013.1.1	148.6-149.4	115.90	7.0	6.2	$0.910 \pm 0.058$	306-1260
Denali183	BE-10015.1.1	165.7-166.6	131.40	10.8	10.1	$0.921 \pm 0.042$	299-971
Denali209*	BE-10016.1.1	187.8-188.7	151.16	9.2	9.8	$0.826 \pm 0.044$	977-1925
Denali210-211	BE-8997.1.1	188.7-190.3	152.29	10.8	20.0	$0.922 \pm 0.033$	327-918
Denali214	BE-10017.1.1	192.1-192.9	155.00	13.7	11.8	$0.831 \pm 0.036$	979-1775
Denali215-216*	BE-8998.1.1	193.0-194.7	156.17	8.8	12.0	$0.925 \pm 0.039$	305-924
Denali217*	BE-10018.1.1	194.7-195.5	157.33	6.7	6.1	$0.731 \pm 0.054$	1890-3351
Denali219-220	BE-8615.1.1	196.4-197.3	159.31	12.0	16.8	$0.841 \pm 0.026$	1001-1539
Denali223	BE-10019.1.1	199.8-200.7	161.93	21.4	17.3	$0.608 \pm 0.029$	3922-4966
Denali224-225	BE-11923.1.1	200.7-202.3	163.06	33.9	17.5	$0.653 \pm 0.010$	3494-3835
Denali228*	BE-10020.1.1	203.5-204.2	165.11	8.7	10.0	$0.627 \pm 0.043$	3415-4861
Denali229-230	BE-11924.1.1	204.2-205.7	166.09	38.6	20.0	$0.691 \pm 0.009$	2972-3326
Denali231	BE-10021.1.1	205.7-206.6	167.18	11.3	11.5	$0.523 \pm 0.037$	5321-6656
Denali232-233	BE-11925.1.1	206.6-208.1	168.26	54.8	30.8	$0.629 \pm 0.008$	3922-4237
Denali234	BE-10022.1.1	208.1-208.8	169.23	9.8 <sup>&amp;</sup>	11.7	$0.378 \pm 0.043$	7740-9894
Denali235 <sup>#</sup>	BE-12465.1.1	208.8-209.4	169.83	20.7	80.3 <sub>DOC</sub>	$(0.437 \pm 0.025)$	$(7043-7999)$
						$0.418 \pm 0.027^{\$}$	$7334-8404^{\$}$

\*Carbon mass  $< 10 \mu\text{g C}$  (excluded for final dating, see main text).

&Carbon mass not significantly  $< 10 \mu\text{g C}$ .

#Results from the DOC fraction.

<sup>\\$</sup>After correction for in-situ  $^{14}\text{C}$  (Fang et al. 2021; see main text)